nature cell biology

Epidermal JunB represses G-CSF transcription and affects haematopoiesis and bone formation

Arabella Meixner[1,3,7], Rainer Zenz[1,4,7], Helia B. Schonthaler[1,6], Lukas Kenner[1,4,5], Harald Scheuch[1], Josef M. Penninger[2] and Erwin F. Wagner[1,6,8]

Mice that lack JunB in epidermal cells are born with normal skin; however, keratinocytes hyperproliferate *in vitro* and on TPA treatment *in vivo*. Loss of JunB expression in the epidermis of adult mice affects the skin, the proliferation of haematopoietic cells and bone formation. G-CSF is a direct transcriptional target of JunB and mutant epidermis releases large amounts of G-CSF that reach high systemic levels and cause skin ulcerations, myeloproliferative disease and low bone mass. The absence of G-CSF significantly improves hyperkeratosis and prevents the development of myeloproliferative disease, but does not affect bone loss. This study describes a mechanism by which the absence of JunB in epithelial cells causes multi-organ disease, suggesting that the epidermis can act as an endocrine-like organ.

The transcription factor activator protein-1 (AP-1) is a dimeric complex that comprises the Jun, Fos, ATF (activating transcription factor) and Maf (musculoaponeurotic fibrosarcoma) protein families[1]. Ubiquitous expression of JunB in mice does not result in an overt phenotype[2], although targeted overexpression of JunB in T lymphocytes interferes with the differentiation of T helper cells[3]. Inactivation of *JunB* was found to cause embryonic lethality at around E9.5 by impairing vasculogenesis and angiogenesis in extra-embryonic tissues[4]. Expression of JunB under the control of the ubiquitin-C promoter (Ubi) prevented death of *JunB* knockout mice (*JunB*$^{-/-}$Ubi–*JunB*). These mutant mice developed myeloproliferative disease (MPD) and had defects in endochondrial ossification, which was also observed in mice lacking JunB[5–7]. JunB negatively regulates the numbers of haematopoietic stem cells and fibroblasts[8,9], controls CBFβ and mTOR, and is translationally regulated in NPM–ALK-positive lymphomas[10,11].

A functional role for JunB–AP-1 in the skin has been proposed for keratinocyte differentiation, carcinogenesis, UV-response and wound repair[12–14]. Epidermis-specific deletion of both *JunB* and *c-Jun* caused alterations of the skin and joints closely resembling lesions of patients with psoriasis[14,15]. Human *JunB* (19p13.2) is localized in the psoriasis susceptibility region PSORS6 and its expression was found to be affected in psoriasis[15]. Thus, downregulation of JunB in the epidermis can be an important factor in psoriasis.

Here we report that mice lacking epidermal JunB (*JunB*$^{\Delta ep}$) are born with normal skin phenotype, although 2–3-month-old mice developed ulcerative skin lesions with MPD and bone loss. JunB represses *G-CSF* transcription and lack of G-CSF in *JunB*$^{\Delta ep}$ mice significantly reduced skin inflammation and prevented MPD development, but did not affect bone loss.

Using the K5-*cre*2 transgenic line[16], we inactivated *JunB* in keratinocytes of mice carrying a floxed *JunB* allele[6] (*JunB*$^{f/f}$, Fig. 1a). Specific deletion of *JunB* in newborn skin was assessed by Southern blotting (Fig. 1b), and was also shown to occur in keratin 5 (K5)-expressing tissues[17] (Supplementary Information, Fig. S1a). The absence of JunB expression in newborn epidermis and cultured primary keratinocytes was verified by western blotting (Fig. 1c, d). Molecular analyses showed that mutant keratinocytes expressed elevated levels of EGFR and cyclin A, whereas expression of the known JunB target gene *p16*^{INK4a} was unchanged (Fig. 1d).

JunB$^{\Delta ep}$ mice were born with the expected Mendelian frequency and were fertile. The architecture and differentiation of newborn *JunB*$^{\Delta ep}$ skin was normal (Supplementary Information, Fig. S2a–f) and no significant epidermal thickening was detected. However, *JunB*$^{\Delta ep}$ keratinocyte proliferation was increased *in vivo* (Fig. 1e–g), and BrdU incorporation by cultured primary *JunB*$^{\Delta ep}$ keratinocytes was doubled (Fig. 1h–j). Treatment of *JunB*$^{\Delta ep}$ adult mice with the tumour promoter TPA (Fig. 1k–p) caused a significant increase epidermal thickening (Fig. 1m) and keratinocyte proliferation (Fig. 1p). Increased proliferation was detected when wild-type keratinocytes were cultured with *JunB*$^{\Delta ep}$ keratinocyte-conditioned medium (Supplementary Information, Fig. S5a). This suggests that growth factors released from *JunB*$^{\Delta ep}$ epidermis can accelerate proliferation of keratinocytes, especially in response to stimuli inducing skin inflammation.

Adult *JunB*$^{\Delta ep}$ mice developed severe skin ulcerations around the nose at 2–3 months of age with 100% penetrance (Fig. 2a, b). They became

[1]Research Institute of Molecular Pathology (IMP), Dr. Bohr-Gasse 7, A-1030 Vienna, Austria. [2]Institute of Molecular Biotechnology (IMBA), Dr. Bohr-Gasse 3, A-1030 Vienna, Austria. Current addresses: [3]Institute of Molecular Biotechnology (IMBA), Dr. Bohr-Gasse 3, A-1030 Vienna, Austria; [4]Ludwig Boltzmann Institute for Cancer Research (LBI-CR), Währingerstraße 13a, A-1090 Vienna, Austria; [5]Institute of Clinical Pathology, Medical University of Vienna, Währingergürtel 18-20, A-1090 Vienna, Austria. [6]Cancer Cell Biology Programme, Centro Nacional de Investigaciones Oncológicas (CNIO), Melchor Fernández Almagro, 3, E-28029 Madrid, Spain. [7]These authors contributed equally to this work.
[8]Correspondence should be addressed to: E.F.W. (e-mail: ewagner@cnio.es)

Received 4 March 2008; accepted 10 June 2008; published online 20 July 2008; DOI: 10.1038/ncb1761

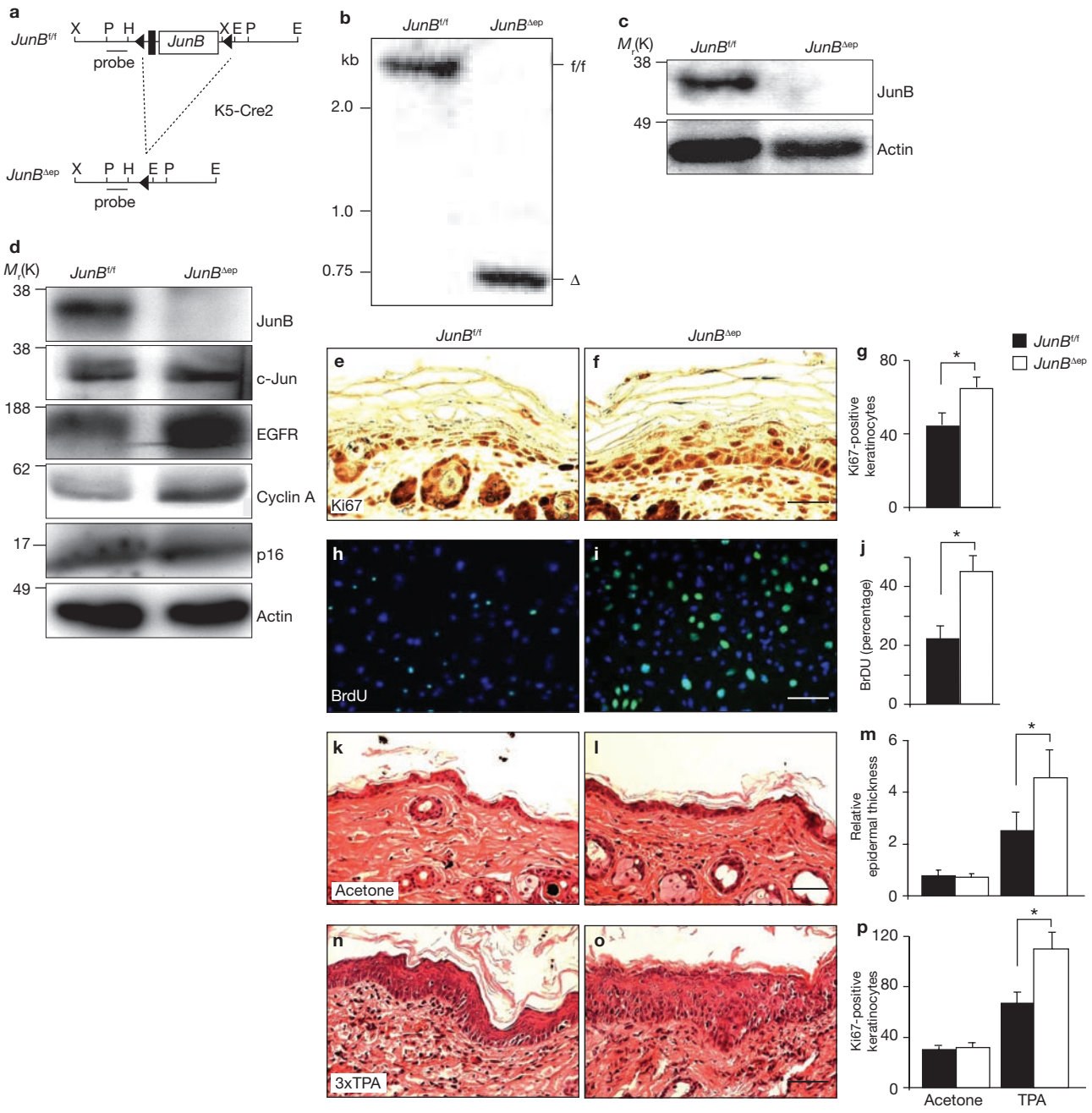

Figure 1 Epithelial-specific deletion of *JunB* induces keratinocyte proliferation and enhances the stress response to TPA. (**a**) Schematic outline of the genomic *JunB* locus before (*JunB*$^{f/f}$) and after Cre-mediated deletion (*JunB*$^{\Delta ep}$). Location of loxP sites (black triangles) and the Southern probe (black bar) are indicated. X, *Xba*I; P, *Pst*I; H, *Hind*III; E, *Eco*RI. (**b**) Southern blot using epidermal DNA showing the floxed (f/f) and deleted (Δ) alleles in the epidermis demonstrating efficient deletion of *JunB* in the epidermis. (**c**–**d**) Western blot analysis confirms the absence of JunB in the epidermis (**c**) and in primary keratinocytes (**d**) of mutant mice. In keratinocytes lacking JunB, EGFR and cyclin A levels were elevated, whereas c-Jun and p16 levels were unaffected (**d**). (**e**–**g**) The number of Ki67-positive keratinocytes was increased in skin from newborn *JunB*$^{\Delta ep}$ mice. (**h**–**j**) A significant increase in the numbers of BrdU-positive cells was observed in primary keratinocytes cultured for four days in the absence of JunB. (**k**–**p**) Adult epidermis was treated with either vehicle (acetone, **k**, **l**) or TPA (**n**, **o**). TPA treatment caused an increase in epidermal thickening (**m**) and keratinocyte hyperproliferation (**p**) in *JunB*$^{\Delta ep}$ mice. Data are mean ± s.d. from five independent experiments (**g**, **j**, **m**, **p**); $^*P < 0.05$, Student's *t*-test. Scale bars are 25 μm (**e**, **f**), 20 μm (**h**, **i**) and 50 μm (**k**, **l**, **n**, **o**). Full scans of gels shown in **b**, **c** and **d** are presented in Supplementary Information, Fig. S7.

moribund by 6 months and died at 8–10 months of age. Skin lesions showed characteristics of epidermal thickening (acanthosis) with pronounced infiltrations of granulocytes, lymphocytes and mast cells (Fig. 2c, d). Mutant mice also had enlarged spleens and lymph nodes containing up to a 10-fold increase in cell numbers (Fig. 2s, t and data not shown). In addition, cellular granulocytes were present in other organs, including the liver (Fig. 2e, f). Marked infiltration of neutrophilic granulocytes in the bone marrow were also observed, indicating the development of MPD (Fig. 2g, h).

At the age of 2–3 months *JunB*$^{\Delta ep}$ mice developed an osteopaenic phenotype (Fig. 2i–r), showing less trabecular bone mass in the tibia metaphysis

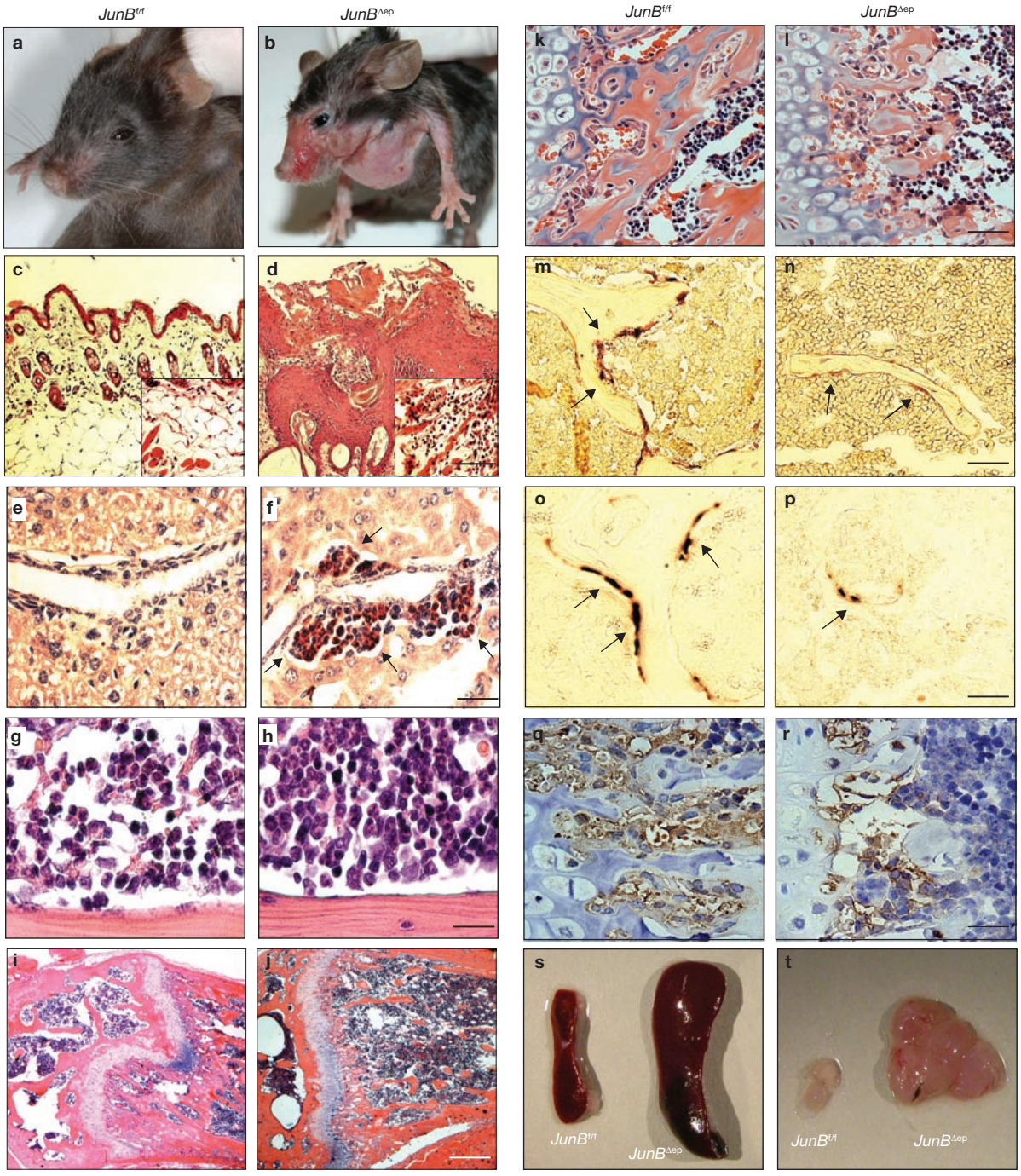

Figure 2 Myeloproliferative disease (MPD) and osteopaenia in *JunB*$^{\Delta ep}$ mice. (**a**–**d**) Three-month-old wild-type mouse with normal skin (**a**) and mutant mouse with ulcerative skin lesions in the face region (**b**), and H&E-stained sections showing wild-type (**c**) and mutant (**d**) epidermal tissue are shown. Hyperproliferative epidermal thickening and inflammatory infiltrates consisting of granulocytes, lymphocytes and mast cells are seen in the mutant tissue. (**e**, **f**) CAE staining of liver sections show marked granulocytic infiltration at different stages of differentiation mutant (**f**, arrows), compared with wild-type (**e**) mice. (**g**–**h**) Effects of epidermal *JunB* depletion on bone. H&E staining of long bone sections show normal wild-type tissue (**g**) and myeloproliferative infiltrates in *JunB*$^{\Delta ep}$ (**h**) mice. (**i**–**l**) Histological analysis (H&E) of the metaphyseal regions (proximal tibia) of wild-type (**i**, **k**) and *JunB*$^{\Delta ep}$ mice (**j**, **l**) at 2 months of age indicates osteopaenia in mutant mice. Trabecular bone mass, stained pink, is diminished in mutant mice. (**m**, **n**) TRAP staining (arrows) of the mutant distal metaphyseal humerus (**n**) shows reduced osteoclast numbers compared with wild-type samples (**m**) from 3–4 months old mice. (**o**–**r**) Detection of the osteoblast marker osteocalcin. *In situ* hybridization for the osteoblast marker osteocalcin (**o**, **p**; arrows) or antibody staining for osteocalcin (**q**, **r**) demonstrates reduced osteoblast numbers in the distal metaphyseal region of 3 months old *JunB*$^{\Delta ep}$ (**p**, **r**), compared with wild-type (**o**, **q**) mice. (**s, t**) *JunB*$^{\Delta ep}$ mice show splenomegaly (**s**) and enlarged lymph nodes (**t**), compared with wild-type mice. Scale bars are 100 μm (**c**, **d**), 50 μm (**c, d,** inset (higher magnification) 25 μm (**e**–**h**, **k**–**r**) , 500 μm (**i, j**).

(Fig. 2i–l), reduced numbers of osteoclasts (Fig. 2m, n) and reduced osteocalcin expression at the RNA (Fig. 2o, p) and protein (Fig. 2q, r) levels, suggesting differentiation defects of osteoblasts. Thus, specific loss of JunB resulted in MPD and bone loss due to osteoblast and osteoclast defects.

The MPD of *JunB*$^{\Delta ep}$ mice was further demonstrated in cytospins of splenocytes and bone marrow cells (Supplementary Information, Fig. S3a–d). Blood smears showed increased numbers of mature neutrophilic granulocytes and platelets, but comparable numbers of eosinophilic granulocytes, erythrocytes and monocytes (Supplementary Information, Fig. S3e, f and data not shown). Comparable levels of *JunB* mRNA and protein were found in Gr-1$^+$/Mac-1$^+$ granulocytes and CD4$^+$ T cells from 3 months old diseased *JunB*$^{\Delta ep}$ and control mice (Supplementary Information, Figs S2h, S3g). Expression of *GM-CSFRα, G-CSFR* and *M-CSFR* was not changed in the Gr-1$^+$/Mac-1$^+$ or bone marrow cells (Supplementary Information, Fig. S2g). These results indicate that the development of the MPD is not a consequence of altered JunB expression in the haematopoietic compartment.

Flow cytometry analysis of moribund mutant mice revealed that spleen, bone marrow and lymph nodes (Supplementary Information, Fig. S3h, i and data not shown) were severely disrupted by mature neutrophilic granulocytes (Gr-1$^+$/Mac-1$^+$). There were fewer B- and T-lymphoid cells and analysis of mutant thymus indicated a loss of single- and double-positive CD4$^+$ and CD8$^+$ T lymphocytes (data not shown).

Lethally irradiated wild-type mice ($n = 8$) received bone marrow cells from control ($n = 4$) or *JunB*$^{\Delta ep}$ mice ($n = 4$) at 4 months of age. Six months after transplantation, the recipients had normal neutrophil counts in the peripheral blood (Gr-1$^+$/Mac-1$^+$ granulocytes: *JunB*$^{f/f}$ 51 ± 11%; *JunB*$^{\Delta ep}$ 50 ± 5%) and had not developed myeloid hyperplasia after seven months. Moreover, these mice had normal numbers of Gr-1$^+$/Mac-1$^+$ granulocytes in the spleen and bone marrow, and normal spleen size (data not shown). This demonstrates that the MPD in *JunB*$^{\Delta ep}$ mice is not transplantable and is probably caused by signals or factors released by the epidermis.

G-CSF levels were markedly increased in sera from *JunB*$^{\Delta ep}$ mice aged 3 and 6 months old, whereas GM-CSF, IL-3, TNFα or IL-4 levels were unchanged (Fig. 3a and data not shown). IL-6 levels were increased in the serum of 6-month-old *JunB*$^{\Delta ep}$ mice (Fig. 3a), indicating that IL-6 is probably not involved in early stages, but rather, at the late stage of the disease. The involvement of the epidermis in the development of MPD was further substantiated by measuring increased G-CSF levels in supernatant from *JunB*$^{\Delta ep}$ primary keratinocytes (Fig. 3b). IL-6 levels were also increased, whereas the secretion of GM-CSF, IL-4, IL-3, TNFα and VEGF was either not changed or not detectable (Fig. 3b and data not shown). These data indicate that in keratinocytes JunB negatively regulates cytokine secretion, especially that of G-CSF, both *in vivo* and *in vitro*.

Proliferation of wild-type splenocytes and bone marrow cells was significantly increased when these cells were grown in conditioned medium from *JunB*$^{\Delta ep}$ keratinocytes, indicating that this effect is related to release of epidermis-derived factors, such as G-CSF (Fig. 3c, d). Indeed, the presence of anti-G-CSF antibodies abolished the proliferative effect of the conditioned medium (Fig. 3e, f). There was no effect *in vitro* of *JunB*$^{\Delta ep}$ keratinocyte-conditioned medium on Thy1.2$^+$ T cells, B220$^+$ B cells or Ter119$^+$ erythrocyte populations (Supplementary Information, Fig. S5b), whereas the number of Gr1$^+$/Mac-1$^+$ granulocytes increased significantly (Fig. 3g). Moreover, increasing concentrations of neutralizing antibodies for G-CSF reduced the proliferation rate of bone marrow cultures to normal levels (Fig. 3h). In contrast, there was no effect of anti-IL-6 on splenocytes or bone marrow proliferation (Fig. 3i). Thus, the proliferative effect on bone marrow and splenocytes can be attributed to G-CSF secreted by JunB-deficient keratinocytes.

Next, we analysed the epidermal contribution of cytokine expression in *JunB*$^{\Delta ep}$ mice by quantitative real-time RT–PCR (qRT–PCR). Expression of *G-CSF* and *IL-6* mRNA was markedly increased in newborn epidermis and in primary keratinocytes from *JunB*$^{\Delta ep}$ mice (Fig. 4a, b) but not altered in either in dermis samples (Fig. 4e) or non-epithelial tissues (Fig. 4c). Expression of *GM-CSF*, *KGF*, *TNFα* and *RANTES* mRNA was unaffected (Fig. 4d and data not shown). Comparison of 6-week-old and 7-month-old *JunB*$^{\Delta ep}$ mice showed no significant differences in *G-CSF*, *IL-6* or *VEGF-A* expression[18] (Supplementary Information, Fig. S6). *JunB* expression, quantified by qRT–PCR and immunohistochemistry, was not reduced in non-epithelial tissues from 7-month-old *JunB*$^{\Delta ep}$ mice (Supplementary Information, Fig S1b and data not shown), suggesting that deletion of *JunB* in kidney, lymph nodes and thymus affected only cell types which do not express JunB. Thus, JunB-deficient keratinocytes are probably the main source of G-CSF and IL-6 secretion.

To test whether JunB can transcriptionally regulate *G-CSF* expression, the G-CSF promoter region was analysed by chromatin immunoprecipitation (ChIP). A typical AP-1 binding site was identified at position –719. Thus, we used *JunB*$^{f/f}$ keratinocytes that were transfected either with adenovirus-GFP (control) or adenovirus-Cre to delete *JunB in vitro.* ChIP in the presence of a specific anti-JunB antibody showed that JunB binds to the *G-CSF* promoter (Fig. 4f). Using a murine *G-CSF* promoter luciferase reporter construct (*G-CSF-luc*), the repression potential of *JunB* was analysed (Fig. 4g). Mutation of the AP-1 binding site at position –719 (G-CSF-mAP-1) abolished the repressive activity. In addition, co-expression of JunB (Ubi-JunB) significantly repressed the basal activity of the luciferase reporter indicating that JunB is indeed a direct repressor of *G-CSF* transcription.

To define the functional role of G-CSF secretion from JunB-deficient keratinocytes, JunB mutants were crossed with mice lacking G-CSF[19]. At 3 months of age *JunB*$^{\Delta ep}$;*G-CSF*$^{-/-}$ mice began to show hyperkeratosis and focal inflammation (Fig. 5a–c), which was significantly milder in double-mutant mice than in the *JunB*$^{\Delta ep}$ mice (Fig. 5d–f). Furthermore, *JunB*$^{\Delta ep}$;*G-CSF*$^{-/-}$ mice did not develop MPD, and spleen sizes and morphology seemed normal (Fig. 5p and data not shown). Cervical lymph nodes were still enlarged and neutrophil counts in blood samples were increased (Fig. 5q; granulocytes: *JunB*$^{f/f}$ 13 ± 5%; *JunB*$^{\Delta ep}$ 59 ± 4%; *JunB*$^{\Delta ep}$;*G-CSF*$^{-/-}$ 36 ± 8%; results are mean ± s.d. of five mice). Bone marrow granulopoiesis was normal in the double-mutant mice (Fig. 5g–i), as were the numbers of myeloid cells (Fig. 5j–l) and mature myeloid cells Gr-1$^+$/Mac-1$^+$ cells in spleen and bone marrow (Fig. 5r, s). Loss of G-CSF did not rescue the bone phenotype and *JunB*$^{\Delta ep}$*G–CSF*$^{-/-}$ mice remained osteopaenic (Fig. 5m–o).

As newborn epidermis and primary JunB-deficient keratinocytes also expressed elevated levels of IL-6, JunB mutant mice were crossed with IL-6-deficient mice[20]. Skin inflammation in these mice was markedly reduced but the myeloproliferation and osteopaenia persisted, suggesting that IL-6 does not have a major role in the development of MPD (data not shown).

The findings described here show that specific deletion of *JunB* in mice using K5-Cre induced high levels of G-CSF expression and multi-organ disease characterized by inflammatory skin lesions, MPD and low bone mass. Genetic inactivation of G-CSF in *JunB*$^{\Delta ep}$ mice improved the skin lesions and prevented MPD development, but had no effect on bone. Juvenile *JunB*$^{\Delta ep}$ mice had normal skin architecture and an increased proliferative response to TPA treatment. Thus, it seems that a specific deletion of *JunB* in cells of the *stratum basale* is not required for

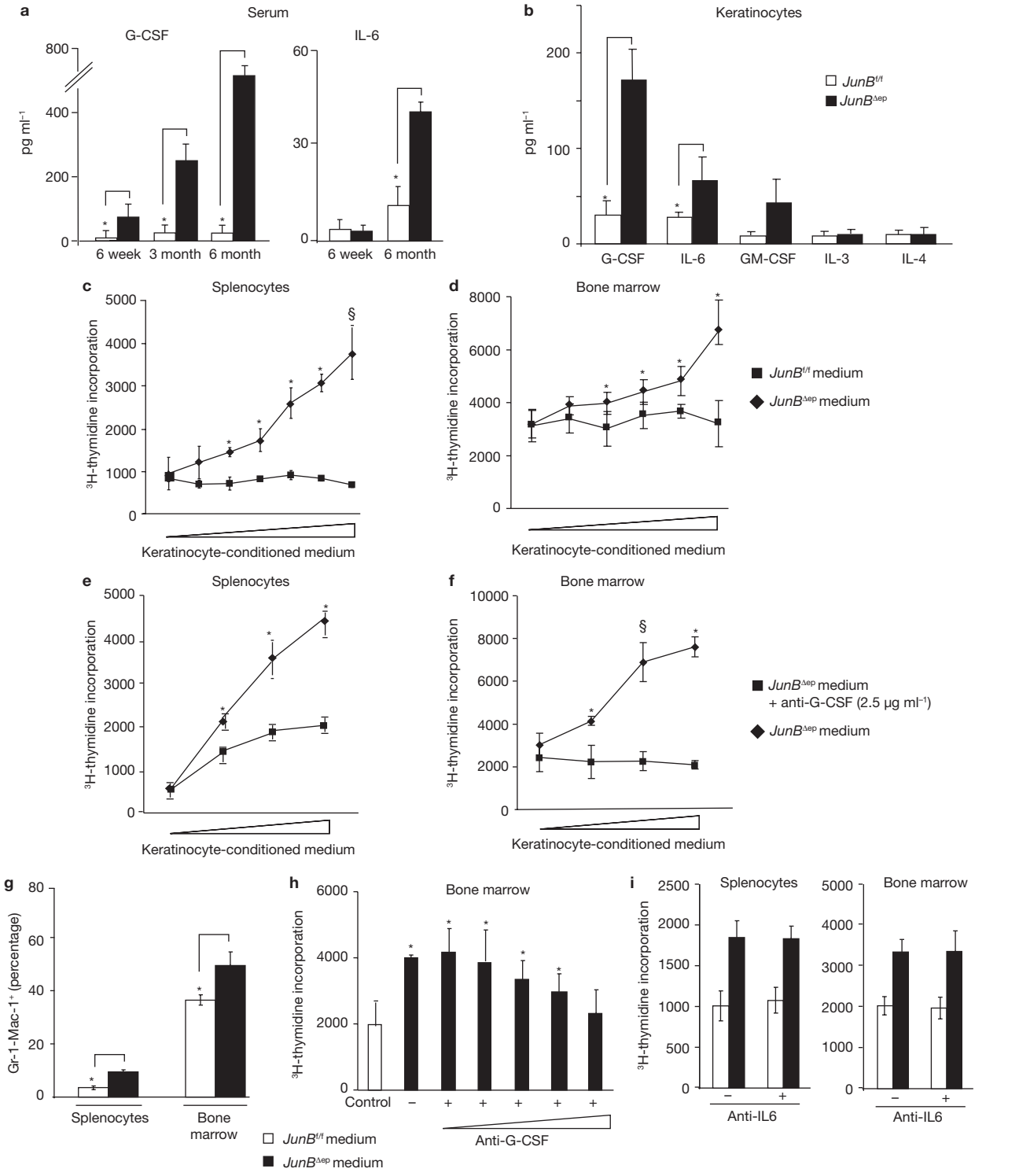

Figure 3 Increased G-CSF expression in *JunB*$^{\Delta ep}$ mice. (**a**) Serum levels of G-CSF were significantly higher in *JunB*$^{\Delta ep}$ than in wild-type mice aged 6 weeks, 3 months and 6 months. IL-6 levels were also significantly increased at the late stage of the disease. (**b**) Primary keratinocytes isolated from newborn *JunB*$^{\Delta ep}$ mice (post-natal day 3) released significantly greater levels of G-CSF and IL-6, compared with wild-type mice. Proliferation of splenocytes (**c**) and bone marrow cells (**d**) from wild-type mice was increased in the presence of increasing amounts of medium from cultured newborn *JunB*$^{\Delta ep}$ keratinocytes (*JunB*$^{\Delta ep}$ medium). No effect on proliferation is observed in the presence of supernatant from control keratinocytes (*JunB*$^{f/f}$ medium). (**e**, **f**) Neutralizing anti-G-CSF antibody (2.5 μg ml^{-1}) significantly reduced proliferation of splenocytes (**e**) and bone marrow cells (**f**) grown in the presence of increasing amounts of *JunB*$^{\Delta ep}$ medium. (**g**) The number of Gr1$^+$/Mac1$^+$ cells was increased in cultures of wild-type splenocytes and bone marrow cells grown in *JunB*$^{\Delta ep}$ medium. (**h**) Increasing amounts of anti-G-CSF antibody (0.01–2.5 μg ml^{-1}) gradually reduced the proliferative effect of *JunB*$^{\Delta ep}$ keratinocyte-conditioned medium on bone marrow cells to control level. (**i**) Anti-IL-6 antibodies had no effect on proliferation of splenocytes or bone marrow cells. For all panels, data are mean ± s.d. from 15 representative littermates (**a**) and from five (**b**) or three independent experiments (**c**–**i**). *$P < 0.05$, §$P < 0.01$ (Student's *t*-test), compared with wild-type or controls.

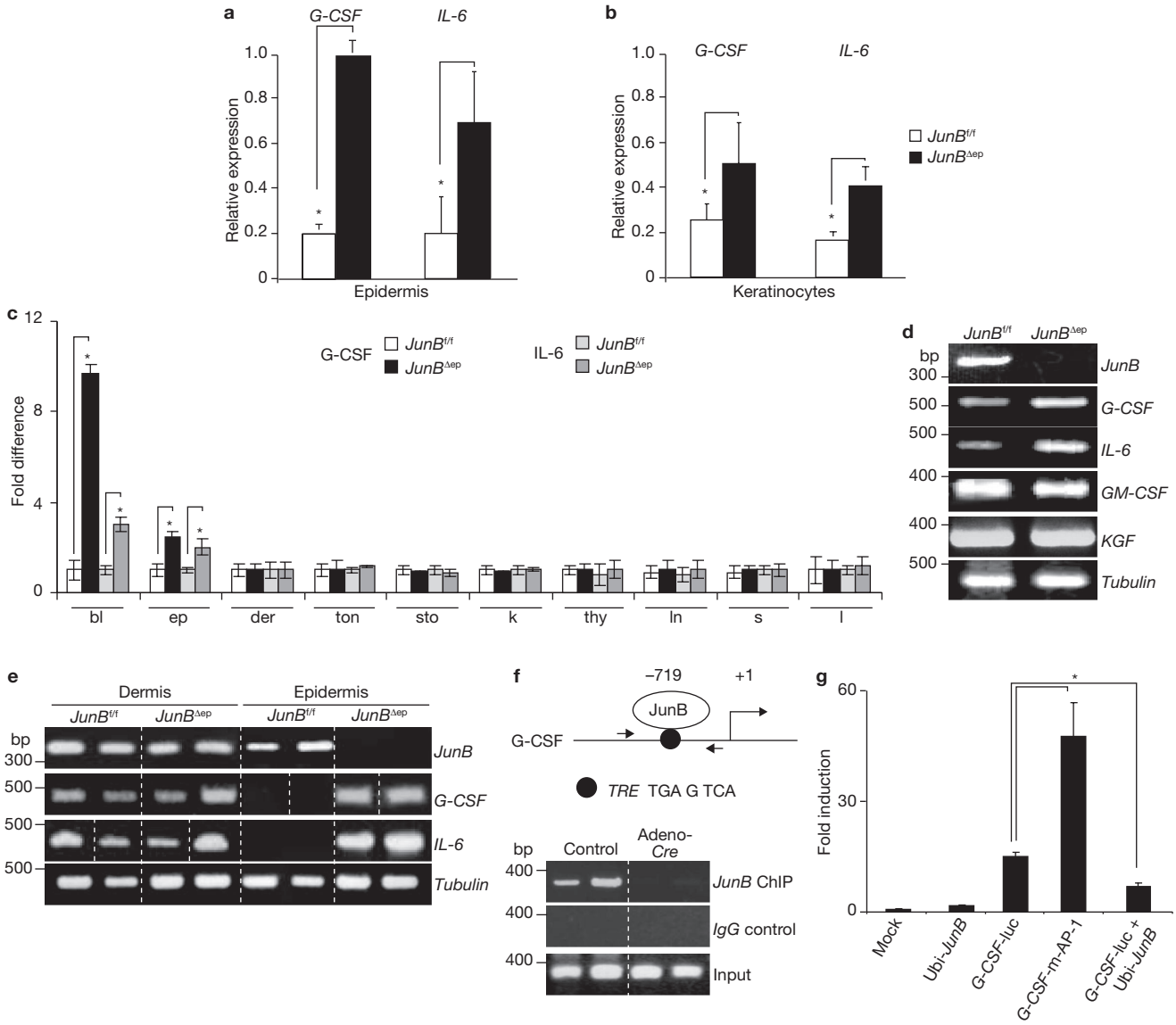

Figure 4 JunB directly regulates *G-CSF* transcription in keratinocytes. (**a**, **b**) qRT–PCR analysis shows increased expression of *G-CSF* and *IL-6* mRNA in epidermis (**a**) and primary keratinocytes (**b**) isolated from newborn *JunB*$^{\Delta ep}$ mice (post-natal day 3) after normalization to tubulin expression. (**c**) G-CSF and IL-6 levels were significantly increased in blood (bl) and epidermis (ep) of *JunB*$^{\Delta ep}$ mice aged 7 months but were not significantly changed in other tissues analysed (bl, blood; ep, epidermis; der, dermis; ton, tongue; sto, stomach; k, kidney; thy, thymus; ln, lymph nodes; s, spleen; l, liver). (**d**) RT–PCR demonstrating the absence of *JunB* expression, elevated expression of *G-CSF* and *IL-6* and unaltered expression of *GM-CSF* and *KGF* in primary mutant keratinocytes. (**e**) Analysis of *JunB*, *G-CSF* and *IL-6* mRNA expression in dermis and epidermis reveals unaltered expression in the dermis of mutant newborns (P3). (**f**) *In silico* analysis of the G-CSF promoter for putative JunB AP-1 binding sites identified a *bona fide* TRE element at position –719 (TGA G TCA), which binds JunB in primary wild-type keratinocytes. Deletion of JunB in *JunB*$^{f/f}$ keratinocytes by adeno–*Cre* transfection prevents specific precipitation. IgG was used as an isotype-specific antibody control and input indicates total cell lysates before immunoprecipitation to ensure equal loading. (**g**) 3T3 cells were transfected with a luciferase reporter plasmid containing no promoter (pGL3, mock), the G-CSF wild-type promoter (*G-CSF*-luc) or the *G-CSF* promoter containing the mutated AP-1 site at position –719 (G-CSF-m-AP-1). Promoter activity 24 h after transfection is shown in relation to the luciferase activity of the vector control, which was set to 1. Co-transfected *Renilla luciferase* reference gene was used for normalization. Mutation of the AP-1 binding site at position –719 increased reporter activity, whereas co-transfection of a *JunB* expression vector (Ubi-*JunB*) reduced the activity of the reporter construct. Data are mean ± s.d. from four (**a**, **b**) or three (**c**–**g**) independent experiments. $^*P < 0.05$ (Student's *t*-test), compared with controls. Full scans of gels shown in **e** and **f** are presented in Supplementary Information, Fig. S7.

epidermal development under physiological conditions, but contributes to the development of multi-organ disease.

The main area affected was the facial skin where pronounced ulcerative lesions developed and infiltration of granulocytes was prominent. G-CSF has not only been shown to promote proliferation of primary human keratinocytes[21] and of HaCaT cells[22], but has also been proposed to be functionally involved in inflammatory neutrophilic dermatoses such as Sweet syndrome[23]. This syndrome has been reported to be associated with leukaemia, including chronic myeloid leukaemia[24], and indicates that high levels of G-CSF can cause inflammatory skin lesions, which may be intensified by persistent mechanical stress from scratching. The *JunB*$^{\Delta ep}$ phenotype could be completely reproduced in adult mice by inducible,

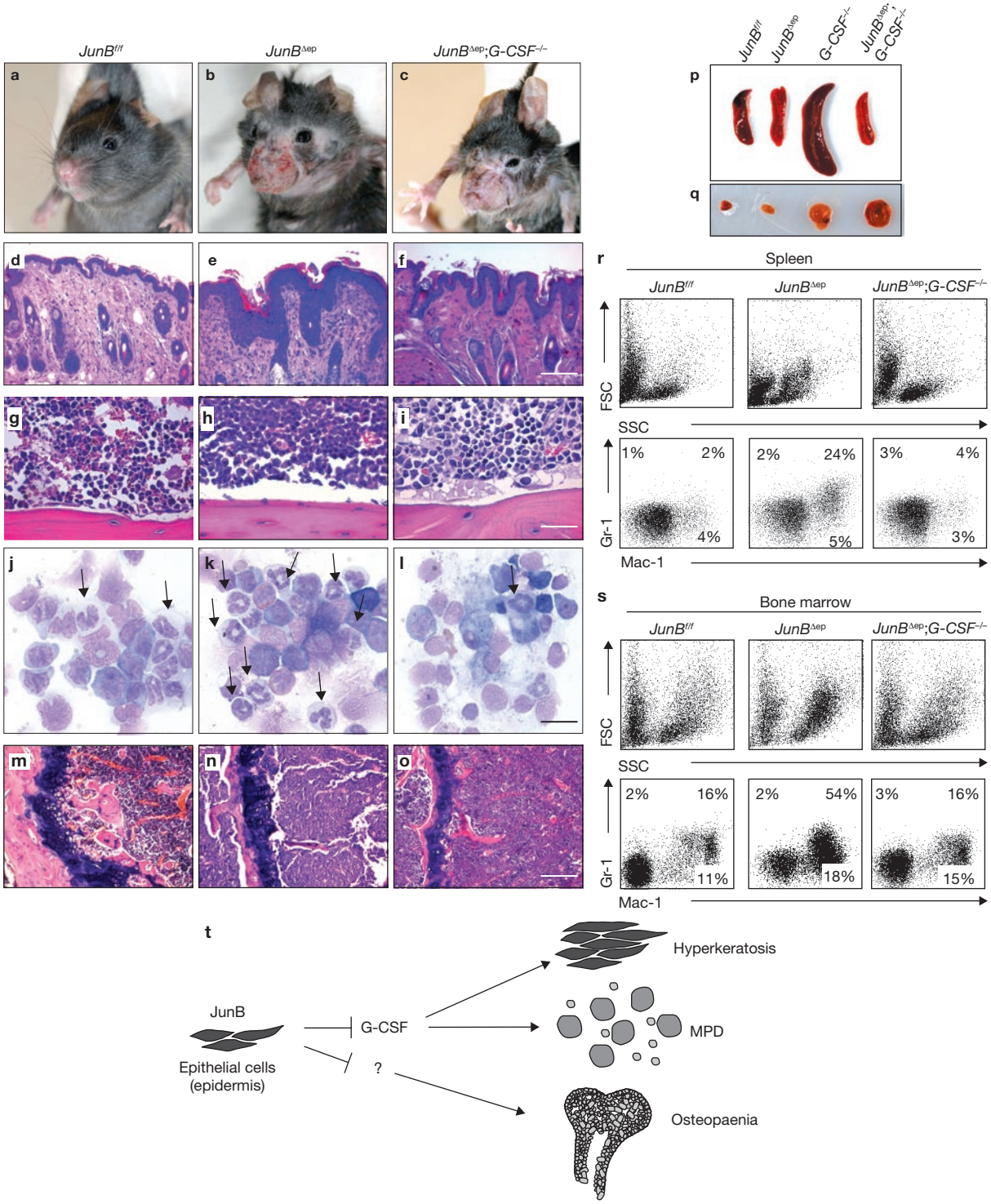

Figure 5 *JunB*$^{\Delta ep}$ mice lacking G-CSF do not develop myeloproliferative disease (MPD). (**a**–**c**) Representative wild-type mouse with normal skin (**a**) and mutant mice (**b**, **c**) with ulcerative skin lesions in the facial region are shown. (**d**–**f**) Representative sections from wild-type mice showing normal epidermis (**d**) and from mutant mice showing hyperproliferative epidermal thickening (**e**, **f**). This was milder in *JunB*$^{\Delta ep}$;*G-CSF*$^{-/-}$ mice. (**g**–**i**) Long-bone sections (H&E) of wild-type (**g**) and mutant mice (**h**, **i**). Myeloproliferative infiltrates are seen in *JunB*$^{\Delta ep}$ mice but not in wild-type or *JunB*$^{\Delta ep}$;*G-CSF*$^{-/-}$ mice. (**j**–**l**) Cytospins of bone marrow cells from 3-month-old wild-type (**j**) and mutant (**k**, **l**) mice. Granulocytes (arrows) and numbers of immature myeloid precursors were unaffected in *JunB*$^{\Delta ep}$;*G-CSF*$^{-/-}$ mice. (**m**–**o**) Histological analysis (H&E) of the metaphyseal regions (proximal tibia) of wild-type (**m**), *JunB*$^{\Delta ep}$ mice (**n**) and *JunB*$^{\Delta ep}$;*G-CSF*$^{-/-}$ mice (**o**) at 3 months of age indicates osteopaenia in double-mutant mice. (**p**, **q**) Splenomegaly (**p**) was not observed, but lymph nodes (**q**) were enlarged in 3-month-old *JunB*$^{\Delta ep}$;*G-CSF*$^{-/-}$ mice. (**r**, **s**) Flow cytometry analyses of single-cell suspensions from spleen (**r**) and bone marrow (**s**) from 3-month-old mice shows that numbers of Gr-1^{+}/Mac-1^{+} granulocytes were unaffected in *JunB*$^{\Delta ep}$;*G-CSF*$^{-/-}$ mice. Numbers in quadrants indicate the average percentage of mice ($n = 4$) per group. (**t**) Schematic model illustrating paracrine and endocrine functions of epithelial cells (epidermis). The absence of JunB leads to high levels of G-CSF in the epidermis and serum. This induces hyperkeratosis and MPD, but does not directly affect the bone. Scale bars, 30 μm (**d**–**f**), 25 μm (**g**–**i**), 500 μm (**m**–**o**).

epidermis-specific deletion of *JunB* (*JunB*$^{\Delta ep*}$) after tamoxifen injection (Supplementary Information, Fig. S4a–o).

The MPD developed rapidly with increased numbers of mature neutrophilic granulocytes (Gr-1$^+$/Mac-1$^+$) present in all haematopoietic organs, but also in non-haematopoietic organs such as liver, lung and kidney. Notably, no hyperproliferation of granulocytes was observed in animals transplanted with bone marrow cells from diseased *JunB*$^{\Delta ep}$ mice, demonstrating a non-cell autonomous disease.

The *JunB*$^{\Delta ep}$ mice also developed a bone phenotype with fewer osteoclasts and osteoblasts expressing reduced levels of osteocalcin. Previous reports have shown that transgenic G-CSF expression or G-CSF injection resulted in increased osteoclast-mediated bone resorption and osteopaenia with infiltration of granulocytes in liver, spleen and lung similar to *JunB*$^{\Delta ep}$ mice[25,26]. G-CSF potently inhibited osteoblast activity by an indirect mechanism resulting in decreased expression of CXCL12–SDF-1 in bone marrow[27]. However, deletion of G-CSF did not affect the bone phenotype. Therefore, the bone loss observed in *JunB*$^{\Delta ep}$ mice may be secondary to the chronic inflammation of the skin. There is substantial epidemiological evidence that many of the chronic inflammatory diseases are associated with systemic bone loss[28].

G-CSF, the primary cytokine controlling the survival, proliferation and differentiation of cells of granulocytic lineage[19] was identified as a JunB target gene in keratinocytes. Culturing wild-type splenocytes and bone marrow cells with *JunB*$^{\Delta ep}$ keratinocytes-conditioned medium resulted in increased proliferation, which could be inhibited by blocking G-CSF but not IL-6. Finally, the loss of G-CSF *in vivo* prevented MPD in *JunB*$^{\Delta ep}$ mice and reduced skin inflammation, whereas in the absence of IL-6 only the skin inflammation was reduced.

Downregulation of JunB in the epidermis of the skin leads to deregulation of cytokine expression, which may be responsible for the endocrine-like role of the skin. Although Southern blot analysis revealed recombination events in non-epithelial tissues, we did not find a reduction of JunB expression in the kidney, lymph nodes or thymus, suggesting that deletion of JunB affects only cells that do not express JunB. Moreover, partial deletion of JunB in K5-positive tissues other than the epidermis did not affect expression levels of JunB, as shown by qRT–PCR , and most importantly, no change in expression of *G-CSF* and *IL-6* was measured. The transplantation experiments further demonstrate that the MPD is not transplantable and therefore not cell-autonomous. In addition, a role of B and T cells in disease development is unlikely, as *JunB*$^{\Delta ep}$ mice in a *Rag2*$^{-/-}$ background still develop the MPD (L.K., unpublished results). We consider a role of thymic epithelial cells in the pathogenesis of the complex phenotype unlikely, although we can not completely exclude it.

Recently it has been shown that the skeleton can exert endocrine functions[29]. Similarly, the skin is not only a natural barrier serving a protective function towards the environment, but also part of the innate immune system[30]. Keratinocytes have been shown to produce factors directly involved in bacterial clearance as well as to attract classical members of the innate immune system such as neutrophilic granulocytes[30,31]. In cases of chronic infections some of these factors, like G-CSF, can reach systemic levels and activate the innate immune system. Under physiological conditions, this defence mechanism is transient and tightly regulated, effectively addressing infection or wounding without causing adverse effects such as chronic inflammation. However, pathological epidermal signalling leads to deregulated cytokine production, for example, through downregulating JunB, thereby affecting organs, such as the haematopoietic system and bone. This study highlights the challenge involved in devising strategies for JunB modulation that would be of benefit in treating human disease. □

METHODS

Generation of *JunB*$^{\Delta ep}$, *JunB*$^{\Delta ep*}$, *JunB*$^{\Delta ep}$;*G-CSF*$^{-/-}$ and *JunB*$^{\Delta ep}$;*IL-6*$^{-/-}$ mice. Mice carrying a floxed *JunB* allele[6] (*JunB*$^{f/f}$) were crossed with the following transgenic lines: 1) mice expressing the Cre recombinase under the control of the keratinocyte-specific *keratin 5* promoter, K5-*cre*2; (ref. 16); 2) mice expressing the Cre recombinase–oestrogen receptor fusion under the control of the keratinocyte-specific *keratin 5* promoter for inducible deletion of *JunB*, K5-*cre*ER^T (refs 15, 32); 3) *G-CSF*$^{-/-}$ (ref. 19) and *IL-6*$^{-/-}$ (ref. 20) mice to obtain double-mutant strains. The genetic background was C57Bl/6/129 for all mice. Tamoxifen was administered as previously described[15].

Southern and western blot analysis. For Southern blots, genomic DNA (10 μg) was digested with *Pst*I to produce a 2.3-kb fragment for the floxed *JunB* allele and a 0.7-kb fragment for the deleted *JunB* allele. For detection of the bands, a 176-bp *Pst*I–*Hind*III fragment of *JunB* was used as a probe as described previously[6]. Western blot analysis was performed according to standard procedures with antibodies specific for c-Jun (Transduction Laboratories), p16, EGFR, cyclin A (Santa Cruz), JunB (M. Yaniv, Institute Pasteur, Paris, France) and actin (Sigma). Antibody dilutions were 1:100 for anti-JunB and 1:1000 for all others. Granulocyte cells were isolated by incubating bone marrow cells with anti-mouse CD11c micro beads (Miltenyi Biotec); T cells were isolated by incubating spleen cells with anti-mouse CD4 micro beads (Miltenyi Biotec). Cells were separated with an auto MACS magnetic cell sorter (Miltenyi Biotec).

Histology and immunohistochemistry. Tissues were fixed overnight with neutral buffered 4% paraformaldehyde at 4 °C and embedded in paraffin. Sections (5 μm) were either stained with haematoxylin and eosin (H&E) or processed further. Immunohistochemistry staining for Ki67 (Novocastra), keratin 5 and keratin 10 (BabCO) was performed with the ABC staining kit (Vector Laboratories) according to the manufacturer's recommendations. CAE (Sigma) staining was performed according to the manufacturer's instructions. For bone analysis, bones were fixed with neutral buffered 4% paraformaldehyde, decalcified for 12 days in 0.5 M EDTA and embedded in paraffin. TRAP-staining of osteoclasts was performed on 5 μm sections using the leukocyte acid phosphatase kit (Sigma). For *in situ* hybridization, sections were deparaffinized and *osteocalcin* mRNA was detected with a probe (provided by C. Hartmann, Institute of Molecular Pathology, Vienna, Austria) using standard procedures. Immunohistochemistry staining for osteocalcin (Santa Cruz) and JunB (N-17; Santa Cruz) was performed with a staining kit (Ventana Discovery). Blood films and cytospins were stained with May-Grünwald and Giemsa solutions (Fluka). Blood counts were determined using an automated animal blood cell-counter (Vetabc, ABX Diagnostics).

TPA-induced hyperproliferation. Eight-week-old littermates ($n = 5$) were shaved and after 24 h treated three times every 48 h with 5 μg TPA or solvent alone (acetone). Forty-eight hours after the last treatment, the back skin was isolated and fixed for histological analysis. Ten high-power fields per back skin were scored for epidermal thickness and Ki67-positive cells.

Flow cytometry. Single-cell suspensions of spleens, lymph nodes or bone marrow cells were prepared and 1×10^6 cells were stained in PBS, 1% fetal calf serum (FCS) and 10 μg ml^{-1} of purified mouse Fcγ III–II receptor antibody with the respective antibodies for 30 min at 4 °C. Monoclonal antibodies were FITC-conjugated (Mac1, B220) and PE-conjugated (c-kit, Gr-1, Thy 1.2; PharMingen).

Cell transplantation. Unfractionated bone marrow cells (1×10^7 cells in 500 μl PBS) were obtained from four-month-old *JunB*$^{\Delta ep}$ mice and injected into the tail vein of 9.6 Gy lethally irradiated recipient mice (C57Bl/6 F1 generation; 12–13 weeks old). Peripheral blood was obtained from the tail vein of each mouse and analysed by flow cytometry and by automated animal blood cell counting.

ELISA. The concentrations of the different cytokines and growth factors in mouse sera, mouse tissues or culture supernatants were measured by ELISA according to the manufacturer's instructions (R&D Systems). Frozen mouse tissues were homogenized using a Precellys24 homogenizer (Bertin Technologies) and 1.4-mm beads in 1% Triton X-100, 10 mM Tris-HCl (7pH .6), 5 mM EDTA, 50 mM NaCl, 30 mM $Na_4P_2O_7$, 50 mM NaF, 200 μM Na_3VO_4, 2 mM PMSF, 5 μg ml^{-1} of aprotinin,

1 μg ml^{-1} of pepstatin A and 2 μg ml^{-1} of leupeptin. The suspension was centrifuged at 12,000*g* for 20 min at 4 °C and the supernatant was stored at –70 °C.

Isolation and culture of mouse keratinocytes. Mouse primary keratinocytes were isolated as previously described[33]. Conditioned medium was collected and filtered (22 μm; Millipore) from primary mouse keratinocyte cultures at day 4. Keratinocyte proliferation was quantified by BrdU incorporation (Becton Dickinson). *JunB*$^{f/f}$ keratinocytes were cultured in the presence of adenovirus Adeno–CRE or Adeno–GFP (control) for 4 days to delete *JunB in vitro*, as described previously[15].

Proliferation assays. Single-cell suspensions of splenocytes or bone marrow cells were prepared from 6–8 weeks old C57Bl/6 mice. For proliferation assays, cells were cultured at 0.5×10^5 cells per well in 100 μl RPMI containing 10% FCS complemented with keratinocyte-conditioned medium, and with or without anti-G-CSF or anti-IL-6 (R&D Systems) as indicated in the figures. Cells were stimulated in quadruplets for 72 h and proliferation was assessed by the ^{3}H-thymidine incorporation added (1 μCi per well) during the last 10 h of culture. Cells were collected using a cell harvester and ^{3}H-thymidine incorporation was quantified by scintillation counting.

RNA isolation and RT–PCR. Total RNA was isolated using the Versagene (RNA Tissue Kit (Gentra System). cDNA synthesis was performed as recommended (Ready-To-Go-You-Prime-First-Strand Beads Kit, Amersham Biosciences). PCR amplifications were performed under standard conditions. Primer sequences for *GM-CSF R*, *G-CSF R*, *M-CSF R*, *GM-CSF*, *KGF* and *tubulin* have been described elsewhere[5,33]. *G-CSFs* 5′- ctgccaccatccctgcctct; *G-CSFas* 5′-ccatctgctgccagatggtggt; *IL-6s* 5′- ttgccttcttgggactgatg; *IL-6as* 5′- ctgaaggactctggctttgt-3′. *VEGF-A-s* 5′- gctgtacctccaccatgcca-3′; *VEGF-A-as* 5′-cgtctgcggatcttggacaa-3′; *JunBs* 5′- agacacaggcgcatctctga-3′; *JunBas* 5′-ctgctgaggttggtgtagac-3′; Expression of gene markers and controls were analysed by real-time PCR using DNA Engine Opticon 2 Lightcycler and iCycler (BioRad). For each sample, expression of the *tubulin* gene was used to normalize the amount of the investigated transcript.

ChIP experiment. Chromatin immunoprecipitations (ChIPs) were performed as recommended (Upstate). The ChIP primers binding in the *G-CSF* promoter region were 5′-ccacgacatcgaggtaatgt-3′ and 5′-cctgtcctcttttcagacccat -3′; JunB antibody (Santa Cruz; N-70) and immunoglobulin G (Santa Cruz) was used as a non-specific isotype control.

Construction of reporter genes and cell transfection. For further details of construction of reporter genes, see Supplementary Information, Methods. For co-expression studies, *Ubi–JunB* plasmid was used as described previously[2]. Immortalized wild-type fibroblasts (passage 30–34) were seeded in 24-well plates one day before transfection at a density of 1×10^5 cells per well in antibiotic-free culture medium. The next day, cells were transfected using lipofectamine as recommended (Invitrogen). Twenty-four hours after transfection, cells were prepared for luciferase assay according to the manufacturer's recommendations (Promega). Luciferase activity was measured using Robion Solaris instrument and analysed using the Solaris program.

Statistical analyses. All experiments were performed at least 3 times. Data in bar graphs represent mean ± s.d. Statistical analyses were performed using non-directional two-tailed Student's *t*-test and P values < 0.05 were considered as significant.

Note: Supplementary Information is available on the Nature Cell Biology website.

ACKNOWLEDGEMENTS

We are very grateful to P. Angel, R. Eferl, D. Maurer, E. Passegué, A. J. Pospisilik, M. Sibilia and J. Guinea Viniegra for critical comments and suggestions to the manuscript; A. Bozec and V. Komnenovic for invaluable support for bone histology, U. Möhle-Steinlein for Southern blots and H. Tkadletz for help in preparing the illustrations. The IMP is funded by Boehringer Ingelheim and this work was supported by grants P14680-Gen and P18478 from the Austrian Research Foundation, by the Research Training Network (RTN) Program of the European Community and part of this work was supported by an FWF Network grant NFN S94-SP11. IMBA is founded by the Ministry of Science and the Austrian Academy of Sciences. JMP is also supported by grants from the Austrian Research Foundation (SFB).

AUTHOR CONTRIBUTIONS

A.M., R.Z., H.B.S. and E.F.W. planned and designed the experiments; A.M., R.Z., H.B.S., L.K. and H.S. performed the experiments; A.M., R.Z., H.B.S., L.K., J.M.P. and E.F.W. analysed and interpreted the data; J.M.P. contributed reagents; A.M., R.Z., H.B.S. and E.F.W. wrote the manuscript.

COMPETING FINANCIAL INTERESTS

The authors declare no competing financial interests.

Published online at http://www.nature.com/naturecellbiology/
Reprints and permissions information is available online at http://npg.nature.com/reprintsandpermissions/

1. Eferl, R. & Wagner, E. F. AP-1: a double-edged sword in tumorigenesis. *Nature Rev. Cancer* **3,** 859–868 (2003).
2. Schorpp, M. *et al.* The human ubiquitin C promoter directs high ubiquitous expression of transgenes in mice. *Nucleic Acids Res.* **24,** 1787–1788 (1996).
3. Li, B., Tournier, C., Davis, R. J. & Flavell, R. A. Regulation of IL-4 expression by the transcription factor JunB during T helper cell differentiation. *EMBO J.* **18,** 420–432 (1999).
4. Schorpp-Kistner, M., Wang, Z. Q., Angel, P. & Wagner, E. F. JunB is essential for mammalian placentation. *EMBO J.* **18,** 934–948 (1999).
5. Passegué, E., Jochum, W., Schorpp-Kistner, M., Mohle-Steinlein, U. & Wagner, E. F. Chronic myeloid leukemia with increased granulocyte progenitors in mice lacking junB expression in the myeloid lineage. *Cell* **104,** 21–32 (2001).
6. Kenner, L. *et al.* Mice lacking JunB are osteopenic due to cell-autonomous osteoblast and osteoclast defects. *J. Cell Biol.* **164,** 613–623 (2004).
7. Hess, J. *et al.* Defective endochondral ossification in mice with strongly compromised expression of JunB. *J Cell Sci.* **116,** 4587–4596 (2003).
8. Passegué, E. & Wagner, E. F. JunB suppresses cell proliferation by transcriptional activation of p16(INK4a) expression. *EMBO J.* **19,** 2969–2979 (2000).
9. Passegué, E., Wagner, E. F. & Weissman, I. L. JunB deficiency leads to a myeloproliferative disorder arising from hematopoietic stem cells. *Cell* **119,** 431–443 (2004).
10. Licht, A. H. *et al.* JunB is required for endothelial cell morphogenesis by regulating core-binding factor beta. *J. Cell Biol.* **175,** 981–991 (2006).
11. Staber, P. B. *et al.* The oncoprotein NPM–ALK of anaplastic large-cell lymphoma induces JUNB transcription via ERK1/2 and JunB translation via mTOR signaling. *Blood* **110,** 3374–3383 (2007).
12. Szabowski, A. *et al.* c-Jun and JunB antagonistically control cytokine-regulated mesenchymal-epidermal interaction in skin. *Cell* **103,** 745–755 (2000).
13. Angel, P., Szabowski, A. & Schorpp-Kistner, M. Function and regulation of AP-1 subunits in skin physiology and pathology. *Oncogene* **20,** 2413–2423 (2001).
14. Zenz, R. *et al.* Activator protein 1 (Fos/Jun) functions in inflammatory bone and skin disease. *Arthritis Res Ther.* **10**, 201 (2008).
15. Zenz, R. *et al.* Psoriasis-like skin disease and arthritis caused by inducible epidermal deletion of Jun proteins. *Nature* **437,** 369–375 (2005).
16. Tarutani, M. *et al.* Tissue-specific knockout of the mouse Pig-a gene reveals important roles for GPI-anchored proteins in skin development. *Proc. Natl Acad. Sci. USA* **94,** 7400–7405 (1997).
17. Byrne, C. & Fuchs, E. Probing keratinocyte and differentiation specificity of the human K5 promoter in vitro and in transgenic mice. *Mol. Cell Biol.* **13,** 3176–3190 (1993).
18. Schmidt, D. *et al.* Critical role for NF-kappaB-induced JunB in VEGF regulation and tumor angiogenesis. *EMBO J.* **26,** 710–719 (2007).
19. Lieschke, G. J. *et al.* Mice lacking granulocyte colony-stimulating factor have chronic neutropenia, granulocyte and macrophage progenitor cell deficiency, and impaired neutrophil mobilization. *Blood* **84,** 1737–1746 (1994).
20. Kopf, M. *et al.* Impaired immune and acute-phase responses in interleukin-6-deficient mice. *Nature* **368,** 339–342 (1994).
21. Kawada, A. *et al.* Granulocyte and macrophage colony-stimulating factors stimulate proliferation of human keratinocytes. *Arch. Dermatol. Res.* **289,** 600–602 (1997).
22. Mueller, M. M. & Fusenig, N. E. Constitutive expression of G-CSF and GM-CSF in human skin carcinoma cells with functional consequence for tumor progression. *Int. J. Cancer* **83,** 780–789 (1999).
23. Kawakami, T. *et al.* Elevated serum granulocyte colony-stimulating factor levels in patients with active phase of sweet syndrome and patients with active behcet disease: implication in neutrophil apoptosis dysfunction. *Arch. Dermatol.* **140,** 570–574 (2004).
24. Liu, D., Seiter, K., Mathews, T., Madahar, C. J. & Ahmed, T. Sweet's syndrome with CML cell infiltration of the skin in a patient with chronic-phase CML while taking Imatinib Mesylate. *Leuk. Res.* **28**, S61–S63 (2004).
25. Kokai, Y. *et al.* Overexpression of granulocyte colony-stimulating factor induces severe osteopenia in developing mice that is partially prevented by a diet containing vitamin K2 (menatetrenone). *Bone* **30,** 880–885 (2002).
26. Lee, M. Y., Fukunaga, R., Lee, T. J., Lottsfeldt, J. L. & Nagata, S. Bone modulation in sustained hematopoietic stimulation in mice. *Blood* **77,** 2135–2141 (1991).
27. Semerad, C. L. *et al.* G-CSF potently inhibits osteoblast activity and CXCL12 mRNA expression in the bone marrow. *Blood* **106,** 3020–3027 (2005).
28. Clowes, J. A., Riggs, B. L. & Khosla, S. The role of the immune system in the pathophysiology of osteoporosis. *Immunol. Rev.* **208,** 207–227 (2005).
29. Lee, N. K. *et al.* Endocrine regulation of energy metabolism by the skeleton. *Cell* **130,** 456–469 (2007).
30. Borregaard, N., Theilgaard-Monch, K., Cowland, J. B., Stahle, M. & Sorensen, O. E. Neutrophils and keratinocytes in innate immunity--cooperative actions to provide antimicrobial defense at the right time and place. *J. Leukoc. Biol.* **77,** 439–443 (2005).
31. Bonizzi, G. & Karin, M. The two NF-kappaB activation pathways and their role in innate and adaptive immunity. *Trends Immunol.* **25,** 280–288 (2004).
32. Brocard, J. *et al.* Spatio-temporally controlled site-specific somatic mutagenesis in the mouse. *Proc. Natl Acad. Sci. USA* **94,** 14559–14563 (1997).
33. Zenz, R. *et al.* c-Jun regulates eyelid closure and skin tumor development through EGFR signaling. *Dev. Cell* **4,** 879–889 (2003).

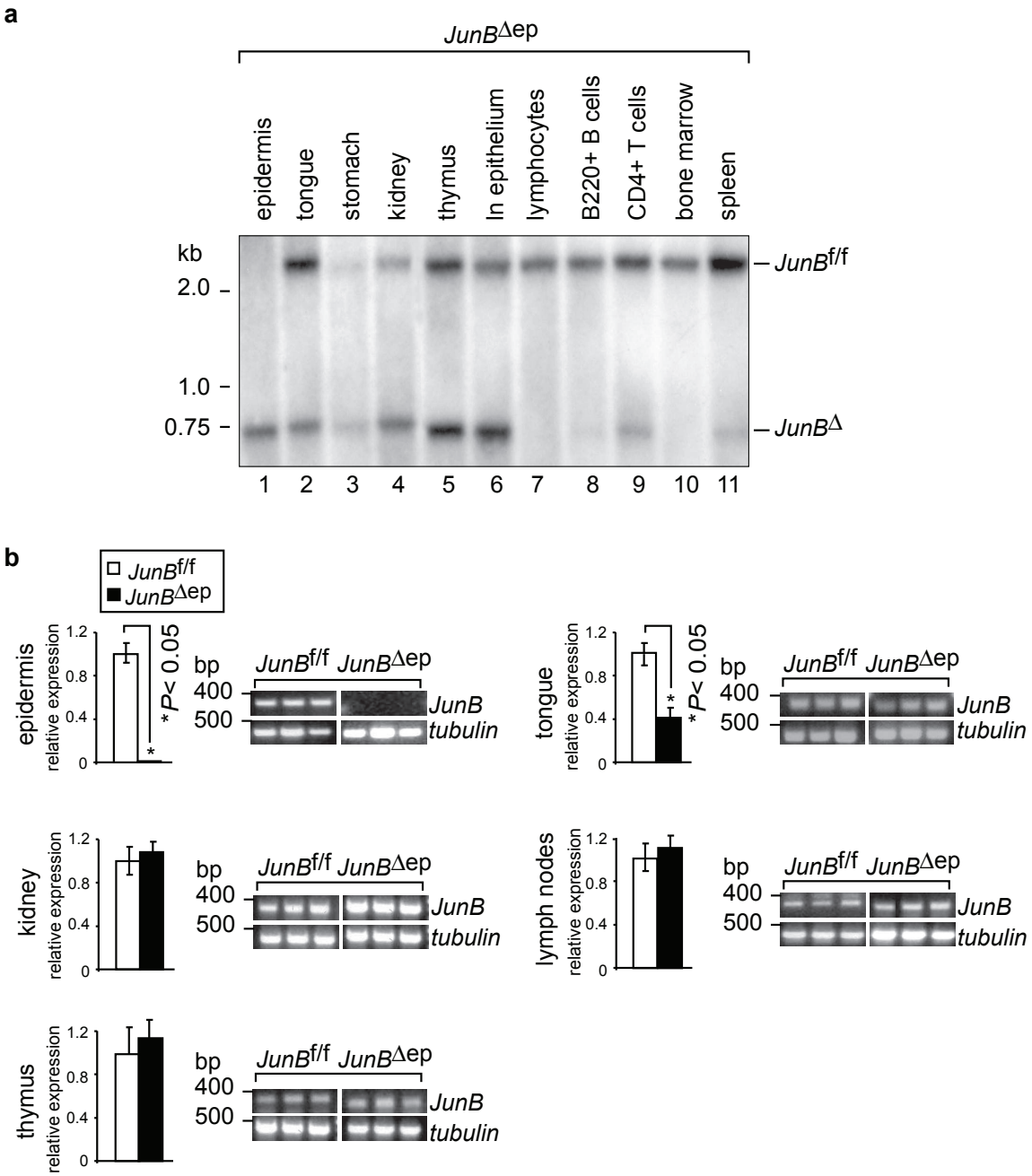

Figure S1 Southern blot analysis and *JunB* expression in various tissues isolated from 7 months old $JunB^{\Delta ep}$ mice. (**a**) Southern blot analyses confirming deletion of JunB ($JunB^{\Delta}$) in the epidermis and Keratin5-expressing tissues (epidermis, tongue, stomach, and thymus epithelium) of $JunB^{\Delta ep}$ mice. Deletion of JunB is also observed in kidney and the epithelium of the lymph nodes (lane 6), but not in lymph node lymphocytes (lane 7). A faint deletion of *JunB* is also seen in B220^{+} B cells, CD4^{+} T cells, and the spleen. No deletion occurred in the bone marrow of $JunB^{\Delta ep}$ mice. (**b**) Expression analyses of *JunB* in various tissues reveals loss of JunB expression in epidermis, a significant downregulation in the tongue, but importantly unaltered *JunB* expression levels in kidney, lymph nodes and thymus. Data are mean ± s.d. from three independent experiments (**b**). Asterisks indicate statistical difference (Student's *t* test) relative to controls.

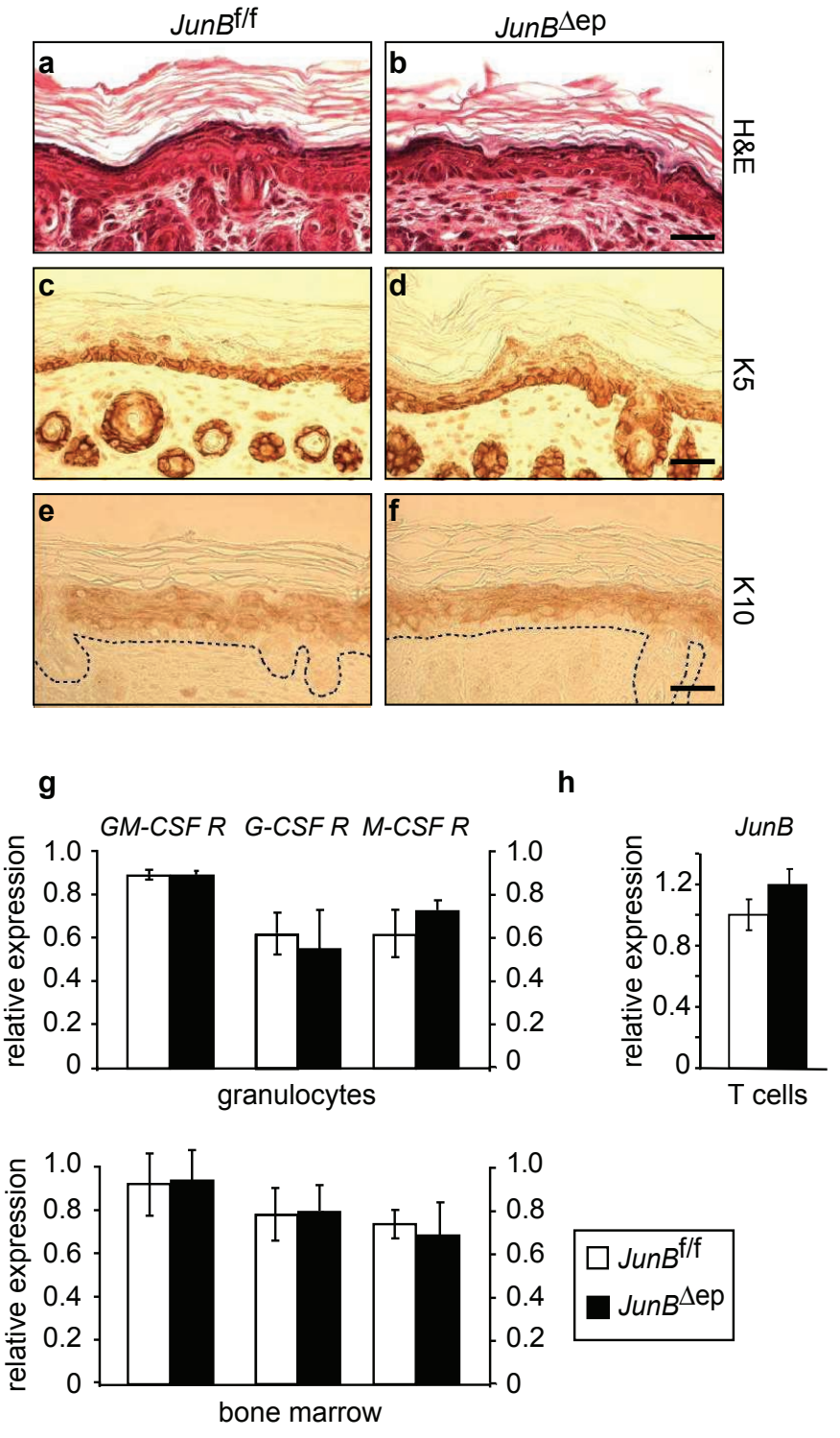

Figure S2 Normal skin architecture in *JunB*$^{\Delta ep}$ mice. (**a, b**) H&E staining and immunohistochemistry for the skin differentiation markers Keratin 5 (**c, d**) and Keratin 10 (**e, f**) of newborn mouse skin (P3) indicates normal architecture and differentiation of mutant epidermis (**b, d, f**). Scale bar, 25 μm. **(g)** qRT-PCR expression analyses for *GM-CSF receptor* (α-chain), *G-CSF receptor*, and *M-CSF receptor* in Gr-1$^+$/Mac-1$^+$ granulocytes (upper panel) and total bone marrow reveals unaltered expression in *JunB*$^{\Delta ep}$ hematopoietic cells of 3 months old mice (n=2). **(h)** qRT-PCR analysis shows normal *JunB* expression in sorted CD4$^+$ T cells of *JunB*$^{f/f}$ and *JunB*$^{\Delta ep}$ mice after normalization to tubulin expression.

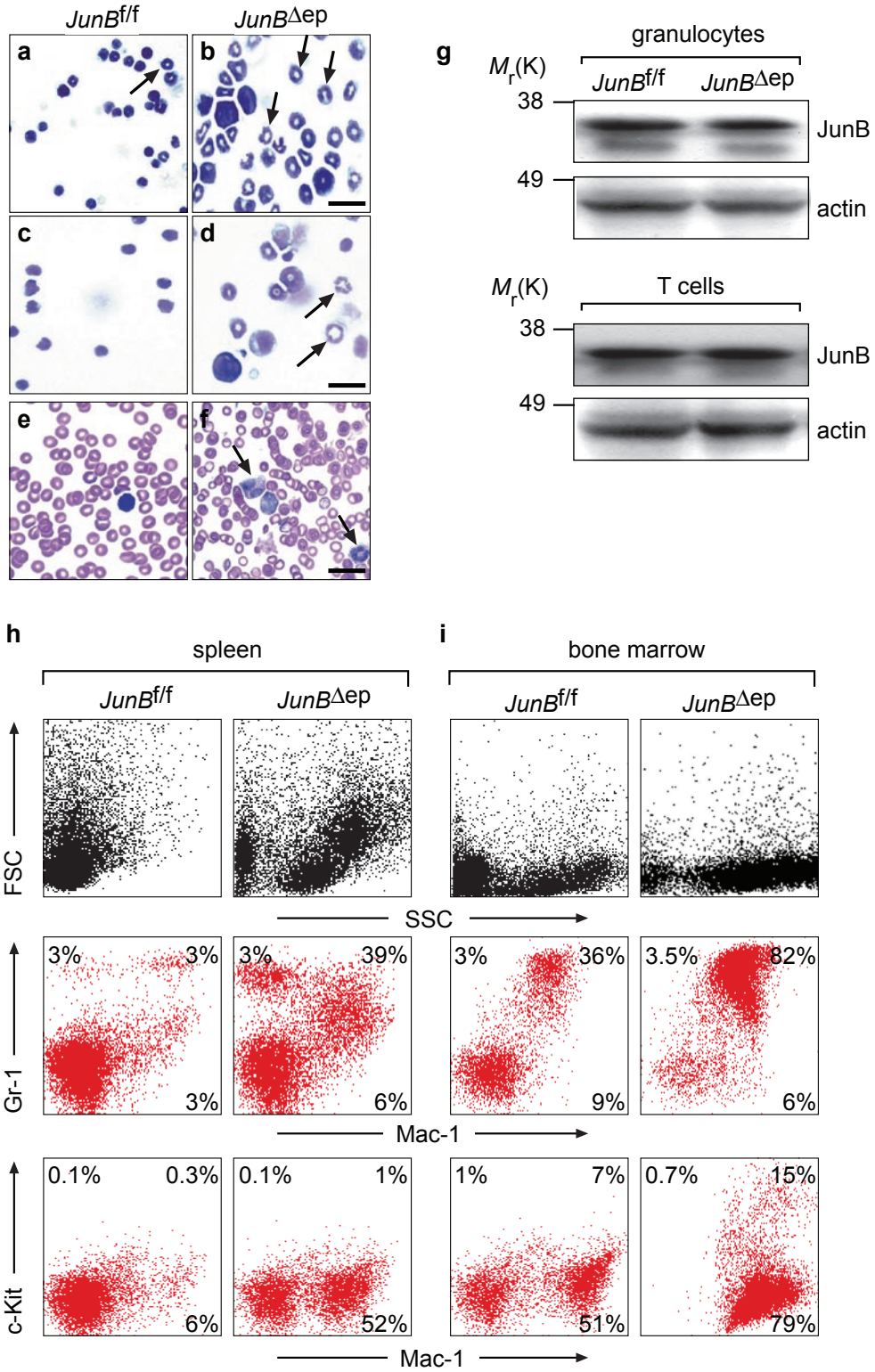

Figure S3 Absence of JunB expression in epithelial cells induces hematopoiesis. Cytospins of splenocytes (**a, b**) and bone marrow cells (**c, d**) from 3 months old mice show accumulation of granulocytes (arrows) and increased numbers of immature myeloid precursors in mutant mice (**b**, **d**). Scale bar, 20 µm. May-Grünwald stained blood smears (**e, f**) show increased numbers of myeloblasts and granulocytes (arrowheads) at the onset of the disease. Scale bar, 30 µm. (**f**). Western blot for JunB of isolated primary Gr-1$^+$/Mac-1$^+$ granulocytes or CD4$^+$ T cells (**g**) demonstrates unaltered expression in *JunB*$^{\Delta ep}$ mice. (**h, i**) Flow cytometric analyses of single-cell suspensions from spleen (**h**) and bone marrow (**i**) from 3 months old mice demonstrating increased numbers of Gr-1$^+$/Mac-1$^+$ granulocytes in *JunB*$^{\Delta ep}$ mice. Numbers in quadrants indicate the average percentage of 4 mice per group.

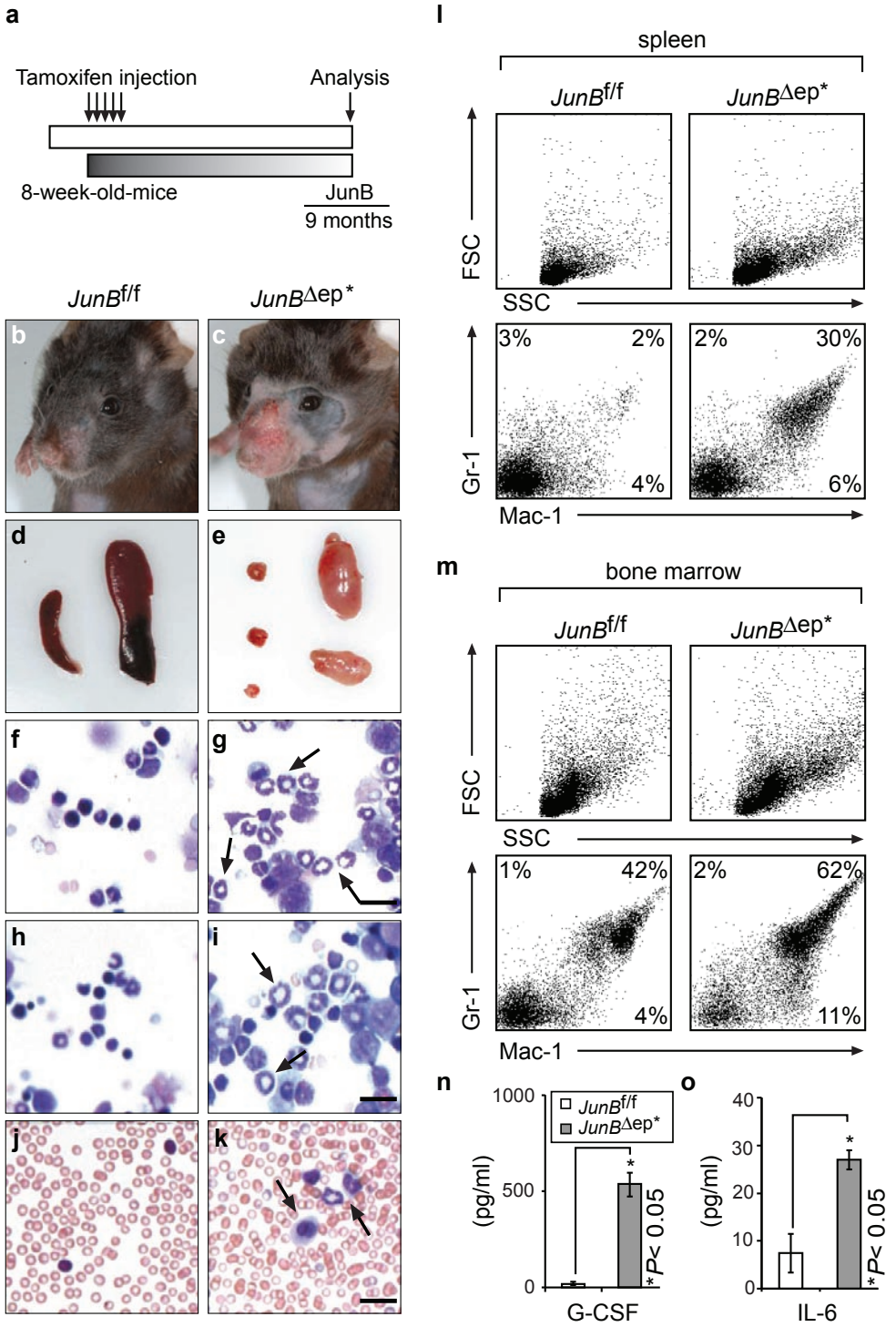

Figure S4 Inducible deletion of *JunB* (*JunB*$^{\Delta ep*}$) in adult mice recapitulates the phenotype of *JunB*$^{\Delta ep}$ mice. (**a**) *JunB*$^{f/f}$ K5-*cre*ER^{T} and control mice (*JunB*$^{f/f}$) were monitored for 7 months after five consecutive injections with tamoxifen (1 mg day^{-1}, intraperitoneal) to induce *JunB* deletion in the epidermis (*JunB*$^{\Delta ep*}$). Ulcerative skin lesions in the face region (**b, c**) and hyperproliferative epidermal thickening with inflammatory infiltrates consisting of granulocytes, lymphocytes and mast cells (not shown), splenomegaly (**d**, right side) and enlarged lymph nodes (**e**, right side) are observed in 9 months old mice. Cytospins of splenocytes (**f, g**) and bone marrow cells (**h, i**) from 9 months old mice demonstrate a strong increase of granulocytes and immature myeloid precursors (**g, i**; arrows). Scale bar, 20 µm. (**j, k**) May-Grünwald stained blood smears showing increased numbers of myeloblasts and granulocytes (arrows) from 9 months aged mice (**l, m**). Scale bar, 30 µm. Flow cytometric analyses of single-cell suspensions from spleen (**l**) and bone marrow (**m**) from 9 months old mice demonstrating increased numbers of Gr-1^{+}/Mac-1^{+} cells in *JunB*$^{\Delta ep*}$ mice. The numbers in quadrant show a representative example of 3 mice per group. ELISA for G-CSF (**n**) and IL-6 (**o**) demonstrates increased G-CSF and IL-6 levels in the serum of *JunB*$^{\Delta ep*}$ mice. Data are mean ± s.d. from four independent littermates (**n**, **o**). Asterisks indicate statistical difference (Student's *t* test) relative to wildtype.

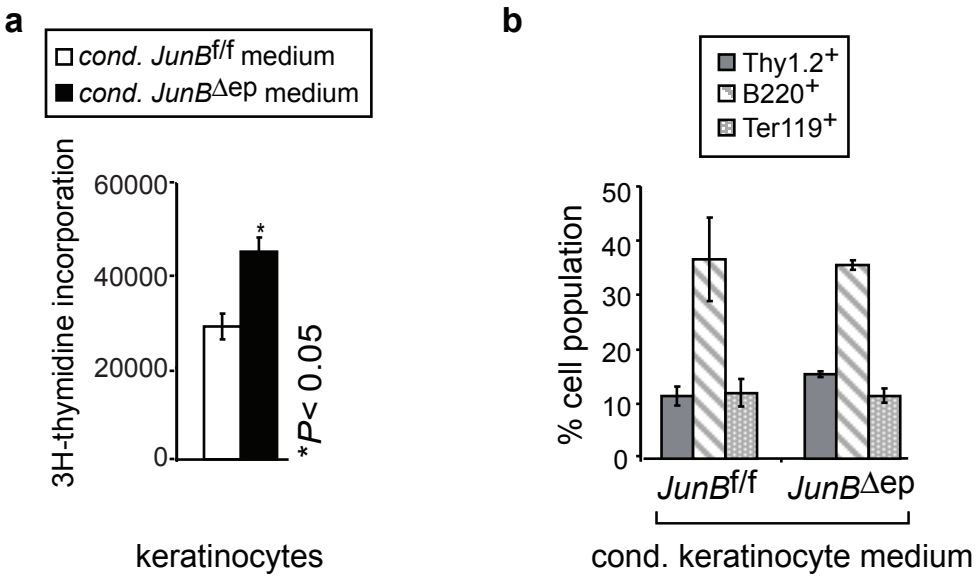

Figure S5 Effects of *JunB*$^{\Delta ep}$ keratinocyte supernatant on immune cells and keratinocyte proliferation *in vitro*. (**a**) Keratinocytes from wild-type mice show increased proliferation in the presence of supernatant from cultured newborn *JunB*$^{\Delta ep}$ keratinocytes. (**b**) No effect on Thy1.2^{+} T cell, B220^{+} B cell or Ter119^{+} erythrocytes population in the presence of supernatant from control or *JunB*$^{\Delta ep}$ keratinocytes. Data are mean ± s.d. from three independent experiments (**a**, **b**). Asterisks indicate statistical difference (Student's *t* test) relative to controls.

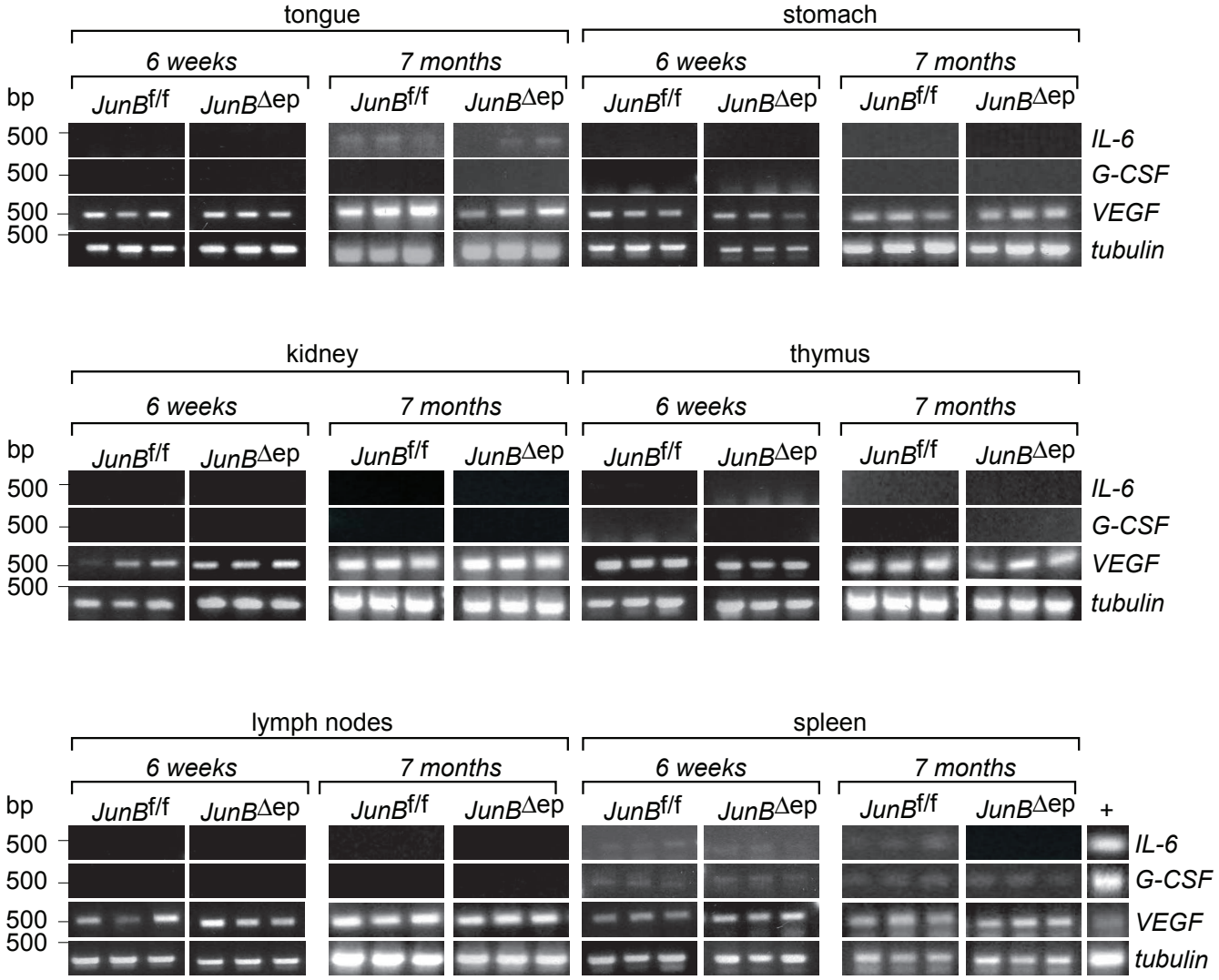

Figure S6 Expression of *G-CSF*, *IL-6* and *VEGF-A* in epithelial tissues isolated from 6 weeks old and 7 months old *JunB*$^{\Delta ep}$ mice. Expression analysis of JunB-dependent target genes *G-SCF, IL-6* and *VEGF-A* in tongue, stomach, kidney, thymus, lymph nodes and spleen reveals unaltered expression levels in 6 weeks and 7 months old *JunB*$^{\Delta ep}$ mice compared to epidermal samples. Epidermis of 7 months old *JunB*$^{\Delta ep}$ mice was used as positive control, +. Experiments were performed in triplicates.

Figure 1b

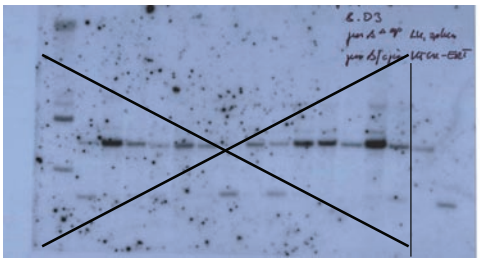

Figure 1c

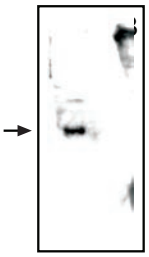

Figure 1d

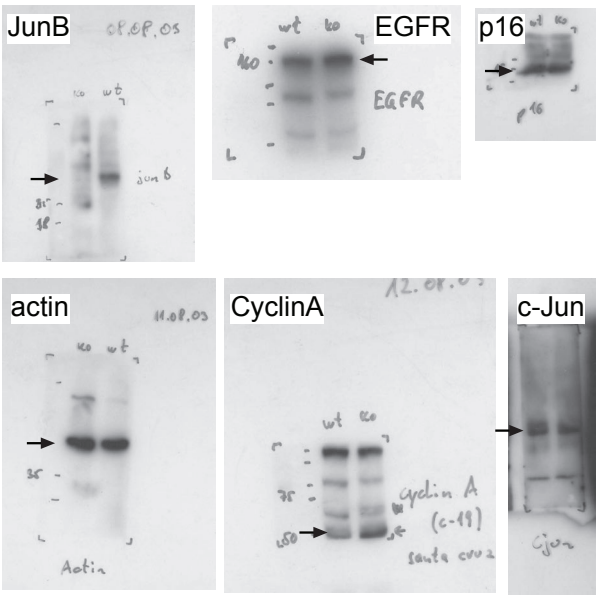

Figure 4e

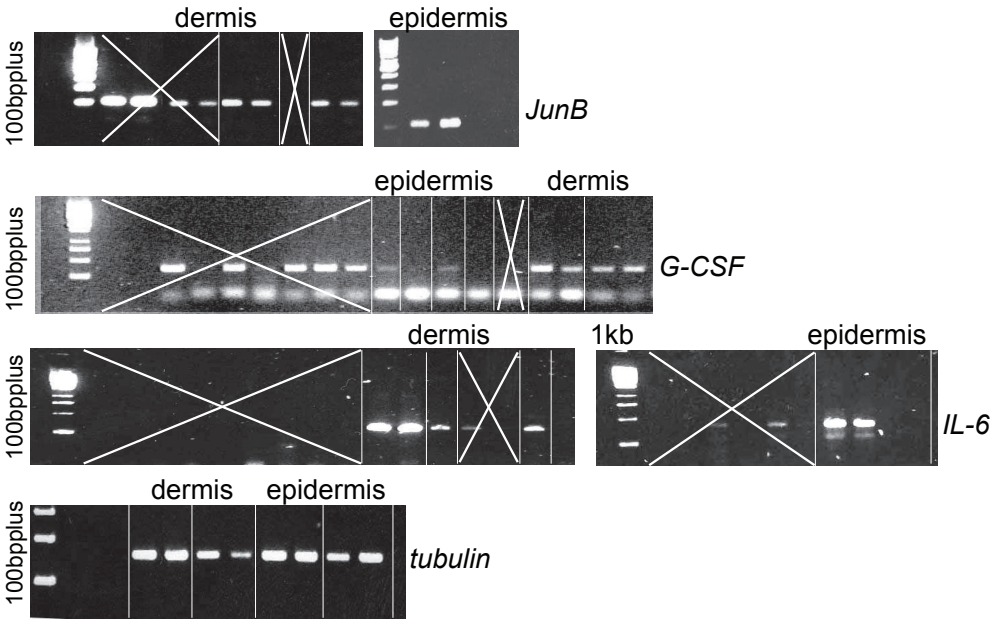

Figure 4f

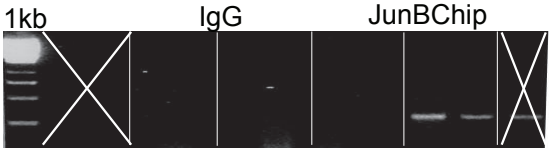

Figure S7 Full scans of key Western and gel data shown in Figs. 1 and 4. Sections relevant for the images shown in the respective figure are marked (line). For PCR gels 1kb or the 100 bp ladder plus were used as MW Standard.

Supplementary Information: Construction of reporter genes

To generate the G-CSF luciferase reporter, a promoter fragment spanning the region –788 to +1 according to the G-CSF sequence (NT_165773.2; 33384931 nucleotides in length; ATG 10103769 nucleotide position) was cloned from genomic mouse DNA by PCR using the following primers: 5'-atgctagcttgattcattcaagacagac-3' and 5'-atgctagcccagggcactcacccattag-3'. The 790 bp fragment was subcloned into TOPO, cut with *Eco*RI, blunt ended and subcloned into *Sma*I site of pGL3 (Promega). Transcription factor binding site was mutated by generating a negative control by PCR using the following primers: (Generation of product A, 800 bp; 5'-a**GGTTCC**taatgggggtattggggagttccc-3' and 5'-atgctagcccagggcactcacccattag-3'; generation of product B, 450 bp 5'-gatgggagatgcagctcctcctttctca-3' and 5'-aagaacctgtcctcttttcagaccca-3'. The negative control was generated using primer 5'-gatgggagatgcagctcctcctttctca-3' and 5'-cttcatgcgcctctgggcagaaagttgag-3'. Finally, the negative control was used to amplify the mutated AP-1 spanning the region from the region –788 to + 1 using primer 5'-atgctagcttgattcattcaagacagac-3' and 5'-atgctagcccagggcactcacccattag-3'. The 790 bp fragment was subcloned into TOPO, cut with *Eco*RI, blunt ended and subcloned into *Sma*I site of pGL3 (Promega). Successful mutagenesis and all PCR fragments were confirmed by DNA sequence analysis.